Available online at www.sciencedirect.com

ScienceDirect

www.elsevier.com/locate/jes

JES JOURNAL OF ENVIRONMENTAL SCIENCES www.jesc.ac.cn

Adsorption of 17β-estradiol from aqueous solution by raw and direct/pre/post-KOH treated lotus seedpod biochar

Ni Liu[1,2], *Yunguo Liu*[1,2,*], *Guangming Zeng*[1,2], *Jilai Gong*[1,2], *Xiaofei Tan*[1,2], *JunWen*[3], *Shaobo Liu*[4,5], *Luhua Jiang*[1,2], *Meifang Li*[1,2], *Zhihong Yin*[1,2]

1. *College of Environmental Science and Engineering, Hunan University, Changsha 410082, P.R. China, E-mail: meet_liuni@hnu.edu.cn*
2. *Key Laboratory of Environmental Biology and Pollution Control, Hunan University, Ministry of Education, Changsha 410082, China*
3. *College of Agriculture, Guangxi University, Nanning 530005, China*
4. *School of Architecture and Art, Central South University, Changsha 410082, China*
5. *School of Metallurgy and Environment, Central South University, Changsha 410083, China*

ARTICLE INFO

Article history:
Received 11 November 2018
Revised 22 May 2019
Accepted 22 May 2019
Available online 11 June 2019

Keywords:
17β-estradiol
Lotus seedpod derived biochar
Activation order
Pre- or post-treatment
Adsorption

ABSTRACT

Five biochars derived from lotus seedpod (LSP) were applied to examine and compare the adsorption capacity of 17β-estradiol (E2) from aqueous solution. The effect of KOH activation and the order of activation steps on material properties were discussed. The effect of contact time, initial concentration, pH, ionic strength and humic acid on E2 adsorption were investigated in a batch adsorption process. Experimental results demonstrated that the pseudo second-order model fitted the experimental data best and that adsorption equilibrium was reached within 20 hr. The efficiency of E2 removal increased with increasing E2 concentration and decreased with the increase of ionic strength. E2 adsorption on LSP-derived biochar (BCs) was influenced little by humic acid, and slightly affected by the solution pH when its value ranged from 4.0 to 9.0, but considerably affected at pH 10.0. Low environmental temperature is favorable for E2 adsorption. Chemisorption, π–π interactions, monolayer adsorption and electrostatic interaction are the possible adsorption mechanisms. Comparative studies indicated that KOH activation and the order of activation steps had significant impacts on the material. Post-treated biochar exhibited better adsorption capacity for E2 than direct treated, pre-treated, and raw LSP biochar. Pyrolyzed biochar at higher temperature improved E2 removal. The excellent performance of BCs in removing E2 suggested that BCs have potential in E2 treatment and that the biochar directly treated by KOH would be a good choice for the treatment of E2 in aqueous solution, with its advantages of good efficiency and simple technology.

* *Corresponding author. E-mail:* liuyunguo_hnu@163.com (Yunguo Liu).

https://doi.org/10.1016/j.jes.2019.05.026
1001-0742 © 2019 The Research Center for Eco-Environmental Sciences, Chinese Academy of Sciences. Published by Elsevier B.V.

Introduction

Nowadays, there is accumulating evidence that water resources have been polluted by endocrine disrupting chemicals (EDCs) (Gorga et al., 2015; Wang et al., 2017b; Zhang et al., 2011a). EDCs are natural or synthetic compounds that have the ability to alter endocrine functions through mimicking or blocking endogenous hormones within the body (Schug et al., 2011). The wide use of pharmaceutical, personal care products and pesticides is directly responsible for the accumulation of EDCs in wastewater (Whitehead and Rice, 2006). In recent years, many research studies have demonstrated that EDCs can have negative impacts on organisms or their progeny, including adverse effects on endocrine function, hormone-dependent cancers, reproductive tract disorders and reduction in reproductive fitness (Pelch et al., 2011; Zhang and Zhou, 2005). Among EDCs, 17β-estradiol (E2) is the major and most potent form of natural estrogens, which has been identified as having the highest endocrine-disrupting activity (Nakada et al., 2004). Meanwhile, it was reported that the transport of natural estrogens like E2 through vegetable cultivation has posed a great threat to the adjacent aquatic environment (Zhang et al., 2015). Therefore, the accumulation and negative impacts of estradiol cannot be ignored, as it may influence the sustainable development of animals and humans. Therefore, how to effectively remove E2 from water and protect our environment and human health has become an urgent problem to be faced.

Adsorption has been proved to be an effective removal method for a multiplicity of pollutants in water (Li et al., 2017, 2018; Worch, 2012) due to its affordable cost and diverse materials, convenient operation and high capacity. Up to now, different adsorbents have been used to remove E2 from water, such as granular or powdered activated carbon, graphene oxide, carbon nanotubes, and molecularly imprinted polymers (Jiang et al., 2016, 2017b; Li et al., 2012; Noir et al., 2007; Sun and Zhou, 2014; Yoon et al., 2003). However, high cost or complicated processing limit their application. With the advantages of abundant feedstock, low cost and favorable physical/chemical surface characteristics, biochar has gained special attention as an adsorbent for water contaminants (Tan et al., 2016c). It has been reported that the feedstock type, as an important factor, could influence the physical and chemical properties of biochar and then affect its removal ability for various pollutants (Ahmad et al., 2014; Tan et al., 2016c). Nowadays, different kinds of cellulose and non-food-based biomass such as bamboo, rice stalk or husk, pinewood, coconut shell, wood shavings and fruit peel have been converted into biochar and applied in environmental management (Tan et al., 2015a, 2015b, 2016b). However, lotus seedpod (LSP), like stalks or hulls, is an abundant agricultural biomass waste resource in Hunan, China, but has not received much attention. Therefore, more attention to LSP biochar and its application potential in water pollution treatment, especially in EDC treatment, is needed.

In order to avoid the limitations of raw biochar, a great deal of research has been carried out to produce engineered/modified biochar with novel structures and surface properties by synthesizing biochar-based composites (Tan et al., 2016c). Activated biochars usually exhibit a great improvement in specific surface area, pore-size distribution and presence of surface active sites, which would make a positive contribution to contaminant removal (Tan et al., 2016c, 2016d; Zeng et al., 2018). Pyrolysis and chemical modification are two common and useful methods to improve material adsorption efficiency. It was reported that biochar pyrolyzed at high temperature exhibited better adsorption performance for E2 in aqueous solution than low-temperature biochar (Wang et al., 2017c), and alkali (KOH) treated biochar presented higher surface area and more excellent adsorption capacity than raw and acid-treated biochar (Liu et al., 2012). Combining the methods of pyrolysis and chemical activation, Tan et al. (2016a) and Huang et al. (2017) used biochar adsorbents prepared by a two-step pyrolysis process with KOH modification to remove organic pollutants, and the produced biochar samples demonstrated good adsorption performance. In addition, pre-treatment of biomass and post-treatment of biochar are the two main approaches for the fabrication of biochar-based materials (Tan et al., 2016c). In recent years, considerable study efforts have been made in comparison of the performance of raw and activated biochar. However, few studies have focused on the structure and property differences between pre-treatment and post-treatment biochar (i.e., the order of modification). Thus, using different types of activated biochar to adsorb E2 is of significance and might provide a more cost-effective approach for E2 removal.

In this study, various LSP-derived biochars (BCs) have been prepared, including raw and KOH-modified biochar, and applied for the removal of E2 in aqueous solution. The main objectives of this work were to: (1) investigate the adsorption capacity of BCs; (2) compare the adsorption capacity between raw and KOH-activated biochar; (3) compare the structure and properties of different modified biochars prepared by direct treatment, pre- or post-treatment with KOH to determine the influence of modification order; (4) examine the impacts of some parameters (i.e., contact time, temperature, pH, ionic strength, humic acid) on the removal of E2 from aqueous solutions; (5) explore the possible mechanisms of E2 removal by BCs. The research results will offer useful information to guide the application of BCs for the removal of E2 in the water environment.

1. Materials and methods

1.1. Materials and reagents

LSPs were collected from a farmers' market in Changsha, Hunan Province, China. E2 (molecular weight 228.29, 98% in purity) was obtained from Sigma–Aldrich (USA). All chemicals were analytical reagent grade and supplied by Shanghai Chemical Corp. Water used in the experiments was deionized water (18.25 MΩ/cm) obtained from a Millipore Milli-Q water purification system.

E2 stock solution (2.5 mg/mL) was prepared by dissolving the solid compound in analytically pure methanol and the standard solution was stored in a refrigerator (below 4°C). Different concentration E2 solutions were prepared by diluting the stock solution with deionized water in later experiments.

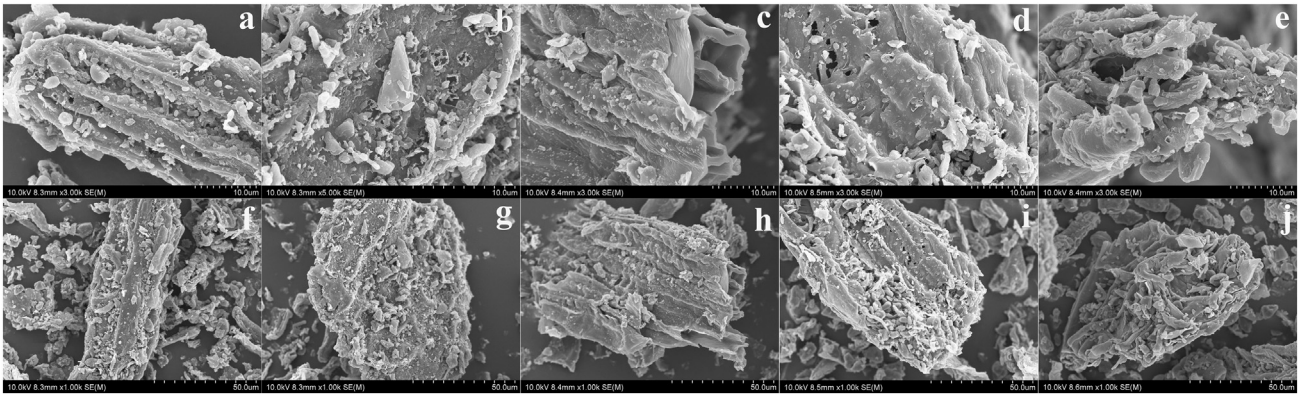

Fig. 1 – SEM images of BCs: (a, f) LSPB, (b, g) LSPB-K, (c, h) KLSP-B, (d, i) LSP400K-B, and (e, j) LSP500K-B.

1.2. *Adsorbent preparation*

BCs were prepared for the adsorption of E2 in water. Firstly, the lotus seeds were taken out of the LSP. Secondly, the materials were washed several times in water to remove ashes and then dried in an air-dry oven (about 60°C). Thirdly, they were pulverized and passed through a 100-mesh sieve (0.147 mm) and stored in clean sealed bags before use.

1.2.1. *Raw biochar*

Ground LSP biomass (15–30 g) was put into a porcelain boat initially. Then, the porcelain boats were placed in a lab-scale tubular reactor (SK-G08123K, Tianjin Zhonghuan Experimental Furnace Co. Ltd., China) to pyrolyze the LSP biomass into biochar. During the pyrolysis process, the tubular reactor was purged using a N_2 flow (50 mL/min) to maintain anoxic conditions, and the reactor temperature was raised to 650°C with a heating rate of 5°C /min. After holding the temperature (650°C) for 2 hr, the reactor was cooled down. Finally, the produced biochar designated as LSPB was collected, and stored in an airtight desiccator before use.

Table 1 – Data for the BET analysis and elemental composition of BCs.

BCs	LSPB	LSPB-K	KLSP-B	LSP400K-B	LSP500K-B
C (%)	69.89	78.85	64.96	77.24	77.63
N (%)	1.12	1.28	0.58	1.25	1.35
H (%)	2.10	2.37	2.51	2.30	2.40
O (%)	15.63	15.11	18.99	15.74	15.14
C/N	62.40	61.60	112	61.79	57.50
O/C	0.22	0.19	0.29	0.20	0.20
(O + N)/C	0.25	0.22	0.33	0.23	0.23
Surface area (m^2/g)	25.21	306.19	227.20	344.42	364.30
Pore size (nm)	2.55	1.94	2.18	2.06	2.17
Pore volume (cm^3/g)	0.03	0.13	0.18	0.38	0.39

BCs: LSP-derived biochar; LSPB: raw lotus seedpod biochar; LSPB-K: direct treated LSPB biochar using KOH; KLSP-B: biochar based on pre-treated LSP biomass using KOH followed by pyrolysis at 650°C; LSP400K-B and LSP500K-B: post-treatment of LSP biochar pyrolyzed at 400 and 500°C using KOH followed by heating at 650°C, respectively.

1.2.2. *KOH-activated biochar*

(1) *Direct treatment of LSPB using KOH (LSPB-K)*

KOH activation was performed on LSPB biochar at room temperature. The modification method was as follows: 500 mL KOH solution and biochar were mixed with 1:5 mass ratio (KOH: biochar), followed by stirring for 2 hr at room temperature. After thorough mixing, the resultant mixture was aged for several hours and the solid was separated from the suspension. The next step was to wash the separated samples with deionized water several times until the pH was neutral. After that, the activated samples were dried at 105°C overnight. The modified samples were stored in air-tight containers and referred to as LSPB-K.

(2) *Pre-treatment of LSP biomass using KOH followed by pyrolysis at 650°C (KLSP-B)*

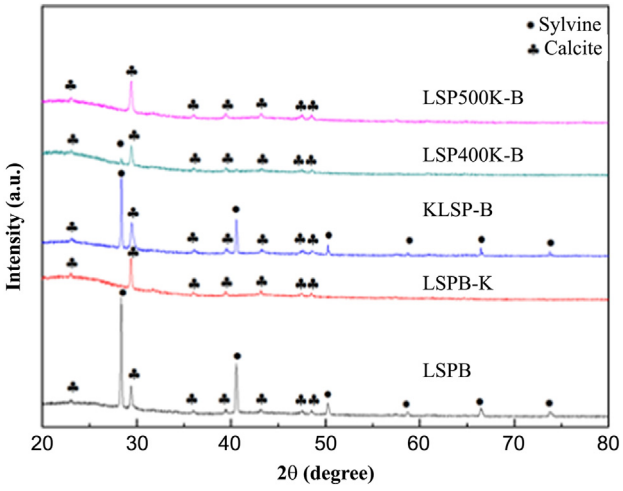

Fig. 2 – XRD patterns of BCs.

KOH activation was performed on the LSP biomass at room temperature. The specific KOH modification method was the same as described in Section 1.2.2 – (1) except that the activation object was LSP biomass; the activated biomass samples are referred to as KLSP. Then, KLSP was pyrolyzed based on the method reported in Section 1.2.1. Finally, the obtained samples were designated KLSP-B.

(3) *Post-treatment of LSP biochar (pyrolysis at 400 and 500°C) using KOH followed by heating at 650°C (LSP400K-B and LSP500K-B)*

Firstly, LSP biomass was converted into biochar at the temperatures of 400 and 500°C for 2 hr in an N_2 environment, respectively. Secondly, the two pyrolyzed biochar samples were treated by KOH, respectively. Thirdly, the obtained activated materials were further heated to 650°C by the pyrolysis method described in Section 1.2.1. Finally, these samples were designated as LSP400K-B and LSP500K-B, respectively.

1.3. Characterization methods

Elemental (C, H, N, O) analyses of adsorbents were conducted using an elemental analyzer (Vario el cube, Elementar, Germany). The BET surface areas and pore structures of adsorbents were determined by N_2 adsorption and desorption measurements (3Flex, Micromeritics, USA). Scanning electron microscopy (SEM) (S4800, Hitachi, Japan) was used to examine the morphologies of samples. X-ray photoelectron spectroscopy (XPS) of samples was carried out with an American Thermo ESCALAB 250Xi XPS System. X-ray powder diffraction (XRD) patterns were obtained on a Rigaku D/Max 2500 diffractometer using CuKα radiation in the scanning range of 20–80° at a scanning rate of 1°/min. FT-IR studies were performed by a spectrophotometer (Nicolet 6700, Thermo Nicolet Co., Waltham, MA, USA) in the wavenumber range of 500–4000 cm^{-1}. For the zeta potential analysis of samples, 3 mg of the adsorbents was added to 50 mL Milli-Q water and the pH (ranging from 4.0 to 10.0) was adjusted with 0.1 mol/L HCl or NaOH. The zeta potential of adsorbents was examined using a zeta potential instrument (Zetasizer, nano-ZS90, Malvern Instruments, Malvern, UK).

1.4. Adsorption experiments

BCs (3 mg) were added into 50 mL E2 solutions of different concentrations. In each experiment, conical flasks were placed in a rotary thermostatic water bath oscillator and shaken for 24 hr at 160 r/min at 27°C. After shaking, all solutions were filtered by 0.45 μm membrane filters. All the experiments were conducted in duplicate.

To analyze the concentrations of filtered E2 solutions, an F-4600 fluorescence spectrophotometer (Hitachi, Tokyo, Japan) was used. During the process, the emission scan mode was chosen, a 450 W xenon lamp served as the excitation source and 700 V was set as the photomultiplier tube voltage. The scan speed was 12,000 nm/min and the excitation and emission matrix spectra were collected at 5 nm intervals. The levels of E2 were investigated by fluorescence detection (λ_{ex} = 290 nm, λ_{em} = 400 nm) and the fluorescence intensity of E2 was collected at Ex/Em = 280/310 nm (Jiang et al., 2016).

The calculation formula of E2 adsorption capacity (q_e) is given in the following equation:

$$q_e = \frac{(C_0 - C_e)V}{m}$$

where, C_0 (mg/L) and C_e (mg/L) are the initial and equilibrium E2 concentrations, respectively; V (L) is the E2 solution volume in the flask, m (g) is the dry mass of the adsorbent.

Batch experiments were carried out to understand the minimum required equilibrium contact time and the effects of relevant factors (temperature, pH, ionic strength and humic acid) on the removal of E2 by BCs. E2 adsorption kinetic studies were carried out by adding 3 mg BCs to E2 solutions (50 mL, 7 mg/L), and then all the samples were shaken for different time periods (5–1680 min). Under different temperatures (290, 300 and 310K), E2 adsorption isotherm studies were performed by following the same procedure used in the kinetic experiments, except that the initial concentration ranged from 1 to 7 mg/L and the shaking time was 20 hr. The impacts of initial solution pH and ionic strength on E2 adsorption were studied under identical conditions to those of the kinetic experiments. The difference was that the pH value of the E2 solutions was adjusted from 4.0 to 10.0 by 0.1 mol/L NaOH or HCl solution and the ionic strength was adjusted by adding various concentrations of NaCl (0, 0.02, 0.04, 0.06, 0.08, 0.1 mol/L) to the E2 solutions. The effect of humic acid was investigated by adding humic acid to E2 solutions (7 mg/L) containing 3 mg BCs. The concentration of humic acid was varied from 0 to 10 mg/L.

2. Results and discussion

2.1. Characterization of adsorbents

2.1.1. SEM and BET analysis

Scanning electron microscope (SEM) images of BCs are presented in Fig. 1, which show the surface structure changes of the biochar after KOH activation. As can be observed, the SEM image of KLSP-B (Fig. 1c) was different from the other samples. It appeared as a square tube structure with a smooth inner wall and a wrinkled surface with few pores. The appearance may be related to the order of KOH activation (i.e., pre-treatment of biomass using KOH followed by pyrolysis). The other four samples present a rougher surface with some insoluble deposited fragments and many different shapes and sizes of pores. Among the BCs, biochar LSPB-K (Fig. 1b) showed the roughest surface and had square pores with different sizes on its surface, which indicated that the direct treatment of LSPB by KOH could enhance its porosity effectively. LSP400K-B and LSP500K-B present inhomogeneous and disordered structures composed of some pores and some lumps of deposits, which may be correlated to the two-step heat treatment.

Brunauer–Emmett–Teller (BET) analysis was used to characterize the texture and pore structure of the adsorbents. The surface area (SA), pore size and pore volume (PV) of the BCs are shown in Table 1. As can be seen, the KOH-activated

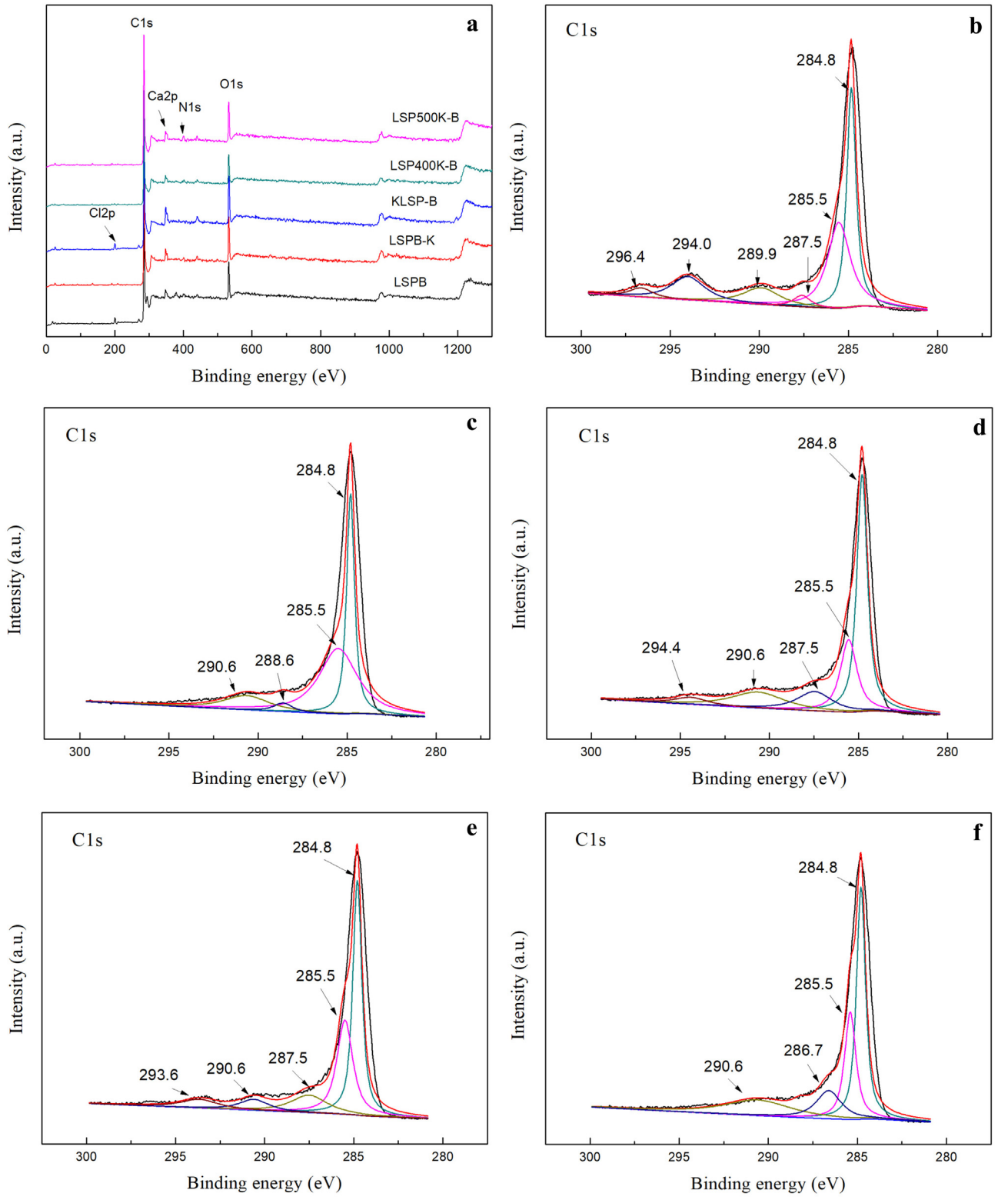

Fig. 3 – XPS analysis of BCs (a) survey spectrum; C1s spectrum of (b) LSPB; (c) LSPB-K; (d) KLSP-B; (e) LSP400K-B; (f) LSP500K-B.

biochar had almost 10 times or even more SA and PV 5 or 10 times that of the raw biochar. This might be attributed to the modification effect of KOH. Among the four KOH-activated biochars, the SA of KLSP-B was relatively lower than that of the other three samples, which indicates that the modification order may have some impact on the SA of biochar. The results of LSP400K-B and LSP500K-B suggested that a two-step modification process and higher pyrolysis temperature might

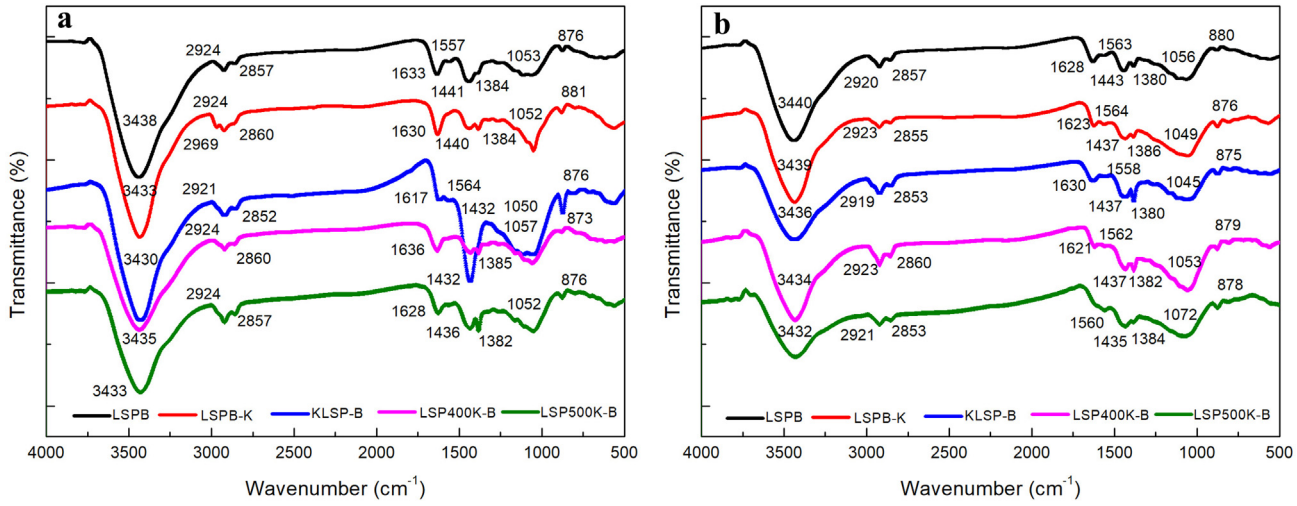

Fig. 4 – FT-IR spectra of BCs (a) before E2 adsorption; (b) after E2 adsorption.

contribute to better development of SA and PV. As exhibited in Appendix A Fig. S1, the N_2 adsorption and desorption isotherms of LSPB, LSPB-K, LSP400K-B, and LSP500K-B corresponded to type II in the IUPAC classification. However, the N_2 isotherm of KLSP-B exhibited a type IV isotherm with a hysteresis loop (H4). The unclosed hysteresis loop of KLSP-B might be ascribed to the increment in desorption potential barriers resulting from the formation of diffusion or chemical traps in the biochar (Zhang et al., 2013).

2.1.2. XRD and XPS analysis

The crystallographic structure of the BCs was obtained using XRD (Fig. 2). Diffraction peaks located at 23.02°, 29.41°, and 35.97°, 39.40°, 43.15°, 47.49°, and 48.51° 2θ were observed on the BCs XRD patterns. These peaks corresponded to planes (012), (104), (110), (113), (202), (018) and (116), respectively, and indicated the presence of calcite ($CaCO_3$) (JCPDS, no. 05-0586). The presence of calcite indicated that alkalinity was plentiful in the raw material (Qian et al., 2016). Meanwhile, some diffraction peaks were observed at 28.35°, 40.51°, 50.15°, 58.64°, 66.38° and 73.73° 2θ only on the LSPB and KLSP-B XRD patterns, which were characteristic of crystalline sylvite (JCPDS, no. 41-1476). The intense sharp peaks at 28.35° and 40.51° indicated that sylvite was well crystallized. However, a small peak at 28.35° 2θ was also been seen on the LSP400K-B XRD pattern. This suggested that raw biochar, pre-treated biochar and biochar processed at the first lower pyrolysis temperature (LSP400K-B) might better maintain the crystalline nature of the LSP material.

The XPS spectrum was measured to gain further understanding of the surface composition of the BCs. Fig. 3 shows the survey and high-resolution C 1s XPS spectra of the BCs. As observed in Fig. 3a, the strong spectrum revealed the existence of C 1s and O 1s at corresponding binding energies (BE) 284.8 and 530.65 eV in the BCs, respectively. A Ca 2p peak at BE at about 346.5 eV was also found in the BCs (Pavón et al., 2005). Moreover, a peak at BE of about 200.11 eV was observed on both LSPB and KLSP-B, which confirmed the presence of Cl 2p (Zhi et al., 2018). The peak located at 530.65 eV in the O 1s XPS spectrum was related to hydroxyl ions (Adhikari et al., 2016). Taking into account the peaks in the high-resolution C 1s XPS spectrum (Fig. 3b–f), common characteristic peaks located at 284.8 and 285.5 eV corresponded to non-oxygenated C and C=N bonds (N-sp^2C type, a defect-containing sp^2 hybridized carbon), respectively (Wang et al., 2001; Yan et al., 2004). The peak centered at 290.6 eV was ascribed to π–π* "shake-up" satellites characteristic of graphite-like carbon (Ismagilov et al., 2009), indicating that graphitic structures could be formed. The peaks at 286.7 and 288.6 eV were assigned to C–N bonds (N-sp^3C configurations, sp^3-hybridized carbon atoms) (Morant et al., 2010; Yan et al., 2004) and C–O bonds (Yan et al., 2004), respectively. The peak appearing at around 287.5 eV could be allocated to –C=O bonds (Okpalugo et al., 2005; Yang et al., 2009). The peak around 289.9 eV could be due to an oxidized C–Ca bond (Andersson et al., 2002). A peak at 294.0 eV in Fig. 3b, which was consistent with those of Fig. 3d and Fig. 3e (at 294.4 eV and 293.6 eV), suggested the presence of $–CF_3$ (Liang et al., 2018; Wang et al., 2017a; Wei et al., 2019). The peak around 296.4 eV was assigned to O–C=O (carboxyl groups) (Gurushantha et al., 2017). The XPS results indicated that the modification by KOH could affect the functional groups on the surface, and might contribute to the development of the graphitic structure of biochar.

2.1.3. Elemental composition

The elemental compositions of BCs are listed in Table 1. Three adsorbents (LSPB-K, LSP400K-B, and LSP500K-B) had similar carbon (C), nitrogen (N) and hydrogen (H) contents. The results indicated that the direct treatment and post treatment methods had little influence on the elemental composition of the biochar. As can be seen, KLSP-B had the lowest content of C and N and the highest H and oxygen (O) content, and C/N, O/C, and (O + N)/C atomic ratios. The C/N ratio of KLSP-B was almost twice that of the other four adsorbents. The atomic ratios C/N, O/C, and (O + N)/C represent the release of inorganic from organic matter, hydrophobicity, and polarity of materials, respectively

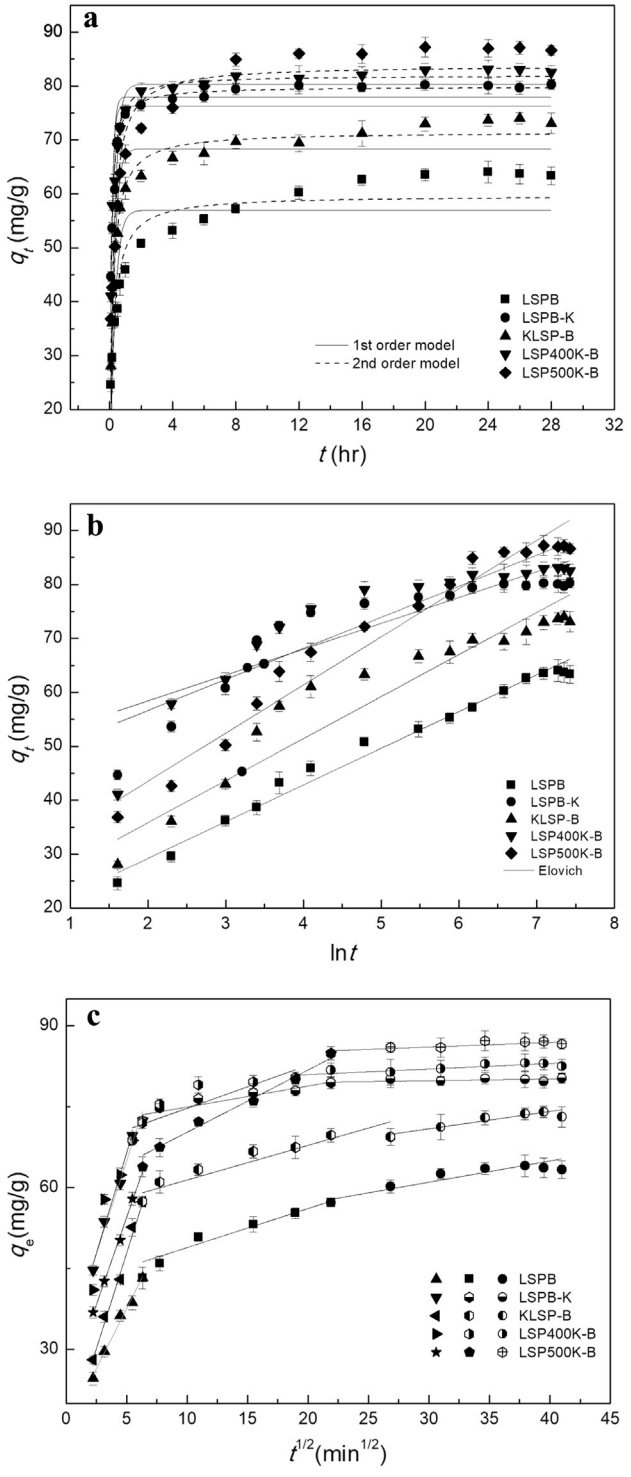

Fig. 5 – Kinetics of E2 adsorption on BCs: (a) pseudo first-order model and pseudo second-order model, (b) Elovich model, (c) Intra-particle diffusion model. Volume 50 mL, adsorbent dose 3 mg, solution concentration 7 mg/L, and agitation speed 160 r/min.

(Zhang et al., 2011b). The result showed that the pre-treated adsorbent (KLSP-B) released more inorganics during preparation and its surface was more hydrophilic. As a polarity index indicator, the (O + N)/C ratio data indicated increased

Table 2 – Kinetic parameters for adsorption of E2 on adsorbents.

Model	parameter	LSPB	LSPB-K	KLSP-B	LSP400K-B	LSP500K-B
Pseudo-first-order	q_e (mg/g)	56.98	76.28	68.38	77.99	80.32
	k_1(hr^{-1})	3.34	8.09	3.88	7.60	3.70
	R^2	0.78	0.81	0.87	0.83	0.78
Pseudo-second-order	q_e (mg/g)	59.67	79.85	71.48	81.97	83.62
	K_2 (g/(mg·hr))	11.95	5.87	11.77	6.70	14.73
	R^2	0.92	0.98	0.97	0.98	0.93
Elovich	α	67.33	128.43	104.99	145.33	158.12
	β	0.15	0.21	0.13	0.17	0.11
	R^2	0.98	0.723	0.92	0.792	0.96

aromaticity and decreased polarity for LSPB-K (Ahmad et al., 2012). The comparative study showed that the KOH modification order had a significant impact on the elemental composition of biochar, as evidenced by pre-treated biochar. However, the effect of the initial pyrolysis temperature was relatively small.

2.1.4. FT-IR spectra

FT-IR spectra of the BCs before and after E2 adsorption are shown in Fig. 4. Generally, all BCs showed the following main characteristic peaks around: 3430 cm^{-1} (hydroxyl –OH), 2920 cm^{-1} (asymmetric vibration of CH_2 groups), 2855 cm^{-1} (symmetric vibrations of CH_2 groups), 1625 cm^{-1} (stretching vibration of aromatic rings and bending vibration of N–H), 1560 cm^{-1} (bending of N–H of secondary amines), 1435 cm^{-1} (–CH_2 symmetric bending), 1380 cm^{-1} (–C–H bending of alkyl groups), 1055 cm^{-1} (CO stretching), and 880 cm^{-1} (bending mode of OH groups) (Abdolhosseinzadeh et al., 2015; Dubey, 2014; Fu et al., 2015; Abo-El-Enein et al., 2017; Shehap, 2008; Wang et al., 2014; Zeng et al., 2015). Compared with the raw biochar (LSPB), it was found that the activated biochars (except KLSP-B) had the same peaks as LSPB. This indicated that most of the functional groups remained on the biochar during the activation process (Regmi et al., 2012). Before adsorption, as seen in Fig. 4a, three differences in the spectrum of KLSP-B compared to the other biochars included two new adsorption peaks that appeared at 1617 and 1564 cm^{-1}, and the absence of the C-H bending of alkyl functional groups (peak around 1380 cm^{-1}). The two notable peaks that appeared in the spectrum of KLSP-B could be ascribed to the bending vibration of –NH_2 groups and the skeletal vibration of aromatic C=C, respectively (Liu et al., 2015; Qin et al., 2002). The reason for this phenomenon might be attributed to the pre-treatment method. A peak around 2969 cm^{-1} was observed in LSPB-K, which was due to the stretching vibrations of aromatic C–H (Li et al., 2015). The peak near 1560 cm^{-1} that represented –NH_2 bending did not appear in the spectra of LSPB-K, LSP400K-B, and LSP500K-B. Combining the characteristics of these samples, it is possible that the process of KOH activation of biochar may cause the breakdown of aromatic structures. After the adsorption of E2 (Fig. 4b), the stretching vibrations of aromatic C-H and the stretching vibration of aromatic rings and bending vibration of N–H disappeared in the spectra of LSPB-K and LSP500K-B, respectively. Meanwhile, the peaks of some functional groups,

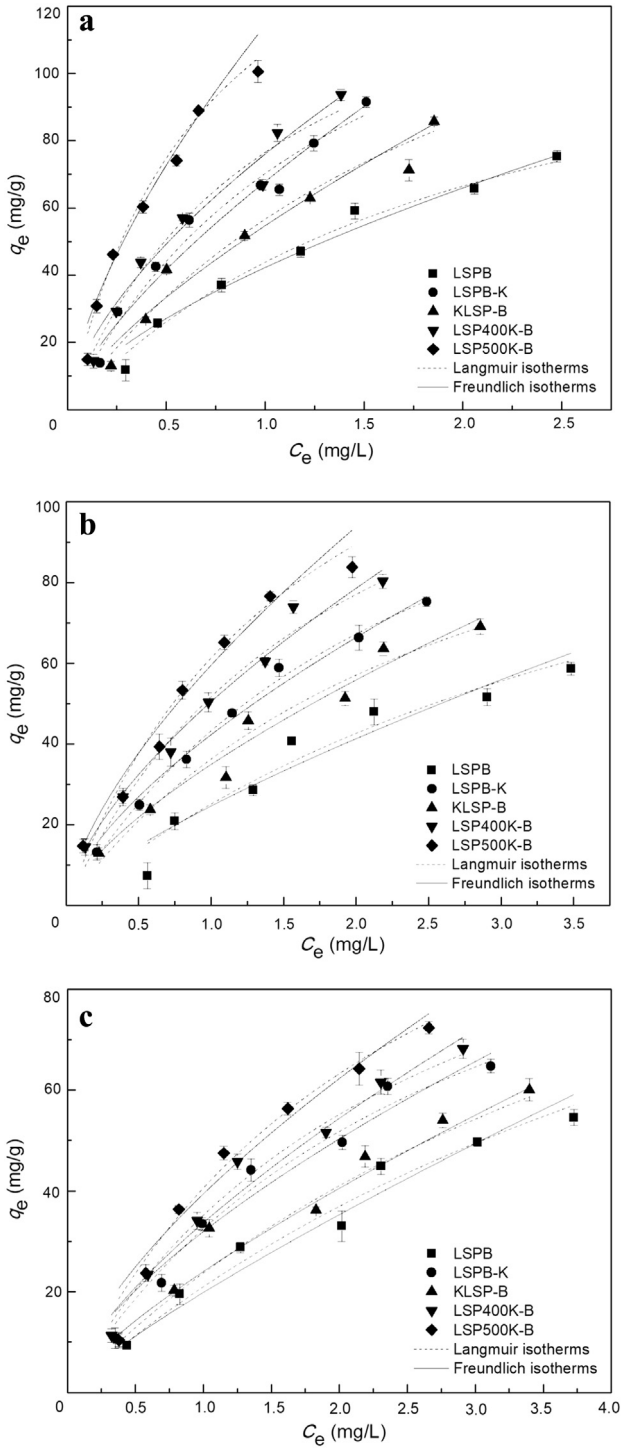

Fig. 6 – E2 adsorption isotherms with BCs at three different temperatures: (a) 290K; (b) 300K; (c) 310K. Volume 50 mL, adsorbent dose 3 mg, solution concentration 1–7 mg/L, and agitation speed 160 r/min.

such as C–H bending of alkyl functional groups, were present in the spectrum of KLSP-B. Through comparison of the spectra of BCs before and after E2 adsorption, it was notable that the adsorption bands shifted from 1052 to 1045 cm^{-1} in LSPB-K and KLSP-B biochar, and 1072 cm^{-1} in LSP500K-B, respectively, indicating the formation of O-C-O groups and aliphatic amines (Janakiraman and Johnson, 2015; Papageorgiou et al., 2010).

2.2. Adsorption kinetics

Adsorption equilibrium studies are important not only for research on adsorption efficiency but also for the exploration of adsorption mechanisms. To understand the potential rate-limiting steps and mechanisms of adsorption, commonly used kinetic models (pseudo first-order, pseudo second-order and Elovich) were used to simulate the experimental data. The model equations are presented in Appendix A Table S1 (Febrianto et al., 2009; Özacar and Şengil, 2005; Weber and Morris, 1963). Fig. 5 and Table 2 show the kinetic experimental results of different models for E2 adsorption onto various adsorbents and the simulated parameters, respectively. It was observed that the capacity of E2 uptake (q_t, mg/g), increased rapidly within the first 2 hr for four adsorbents (LSPB, LSPB-K, KLSP-B, and LSP400K-B). However, the initial rapid uptake of E2 by LSP500K-B lasted almost 8 hr and the adsorbed amount was higher than that of the other four adsorbents at this time. This may be related to the larger surface area (364.30 m^2/g) and pore volume (0.39 cm^3/g) and abundant activated sites of LSP500K-B. After shaking for 8 hr, the adsorption capacity of all adsorbents increased slowly and tended toward equilibrium at 20 hr. Hence, 20 hr was chosen as the reaction time in the following experiments.

As illustrated in Table 2, the pseudo second-order model fitted the data best, as the correlation coefficient (R^2) was much higher than those of the pseudo first-order and Elovich models. Meanwhile, the calculated q_e values were closer to the experimental q_e, further indicating the feasibility of the pseudo second-order model to fit the kinetic E2 adsorption results. This trend indicated that the rate-limiting step was chemisorption, involving valence forces through the sharing or exchange of electrons between adsorbent and adsorbate, by complexation, coordination and/or chelation (Febrianto et al., 2009).

To further investigate the mass transfer steps in E2 adsorption, the intra-particle diffusion model (Appendix A Table S1) was applied. As shown in Fig. 5c, the plots of q_t versus $t^{1/2}$ of BCs were multi-linear, which suggested that three steps took place in the adsorption process. The first portion with a sharp curve might be due to the diffusion of E2 through the solution to the external surface of the adsorbent, or the boundary layer diffusion of solute molecules. The second portion represented the gradual adsorption stage, where intra-particle diffusion (from the external surface into the pores of BCs) was the rate-limiting step. The third portion was the final equilibrium stage. Due to the extremely low E2 concentration left in the solution, the intra-particle diffusion started to slow down and reach saturation at this stage (Cheung et al., 2007). Therefore, a conclusion may be drawn that the diffusion process included film diffusion and intra-particle diffusion, and the rate limiting stage was controlled not only by intra-particle diffusion, but was also related to the pore size of the adsorbents and concentration of E2 in solution. Similar results were reported in a previously published article (Jiang et al., 2017a).

Table 3 – Isotherm model parameters of E2 adsorption by BCs at three temperatures.

BCs	Temperature	Langmuir			Freundlich		
		q_m (mg/g)	K_L (L/mg)	R^2	K_f (L/mg)	n	R^2
LSPB	290K	147.116	0.418	0.982	41.906	0.676	0.961
	300K	135.740	0.226	0.929	24.610	0.733	0.903
	310K	120.917	0.225	0.969	22.296	0.709	0.960
LSPB-K	290K	163.687	0.760	0.967	68.463	0.661	0.963
	300K	150.104	0.405	0.994	41.938	0.670	0.986
	310K	131.440	0.329	0.973	31.701	0.680	0.951
KLSP-B	290K	156.231	0.565	0.956	54.013	0.670	0.947
	300K	147.461	0.311	0.955	34.601	0.683	0.949
	310K	126.370	0.263	0.964	26.097	0.696	0.960
LSP400K-B	290K	167.177	0.850	0.968	75.367	0.658	0.963
	300K	156.584	0.495	0.974	50.338	0.646	0.970
	310K	131.877	0.369	0.984	34.456	0.669	0.968
LSP500K-B	290K	183.600	0.300	0.982	88.444	0.649	0.962
	300K	164.131	0.568	0.975	57.480	0.644	0.963
	310K	154.533	0.341	0.967	37.874	0.707	0.942

2.3. *Adsorption isotherms*

Adsorption isotherm models are fundamental characteristics and mathematical derivations (Foo and Hameed, 2010), and are significant for understanding the mechanisms of adsorption. Two widely used isotherm models (Langmuir and Freundlich) were used to fit the adsorption data. The isotherm model equations are shown in Appendix A Table S2 (Shin et al., 2011). The various isotherm results and all model parameters of E2 adsorption by BCs are presented in Fig. 6 and Table 3, respectively. As shown in Fig. 6, the adsorption capacity of E2 by BCs increased with increasing E2 concentration at all tested temperatures. The adsorption capacity of E2 onto BCs declined with the rise of temperature, which indicated that lower environmental temperature would be good for removal of E2 by BCs and that the adsorption process might be spontaneous (Yan et al., 2017). The R^2 values listed in Table 3 are the determination coefficients of the isotherm models. According to the value of R^2, the Langmuir model showed a better fit than the Freundlich model, which demonstrated that E2 adsorption by BCs took place in a monolayer fashion (the adsorbed layer was one molecule in thickness), and adsorption could only occur at a fixed number of definite localized sites, without lateral interaction and steric hindrance between adsorbed molecules, even on adjacent sites (Vijayaraghavan et al., 2006). In its derivation, the Langmuir isotherm assumes that each molecule possesses constant enthalpy and adsorption activation energy, with no transmigration of the adsorbate in the plane of the surface, and is referred to as homogeneous adsorption (Foo and Hameed, 2010).

2.4. *Effect of solution pH*

pH is a significant influencing factor in adsorption because it affects the surface charges of adsorbent samples and the ionization of chemical species (Zhang and Zhou, 2005). The effect of initial pH on E2 adsorption by BCs with pH ranging

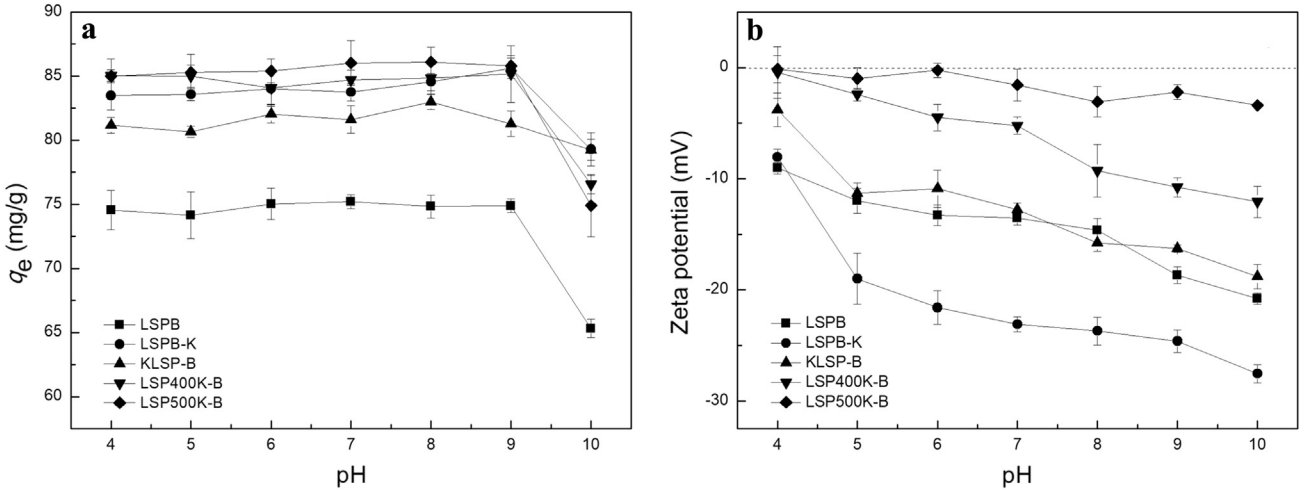

Fig. 7 – (a) Effects of solution pH on E2 adsorption by BCs; (b) Zeta potential of BCs at different pH. Volume 50 mL, adsorbent dose 3 mg, solution concentration 7 mg/L, and agitation speed 160 r/min.

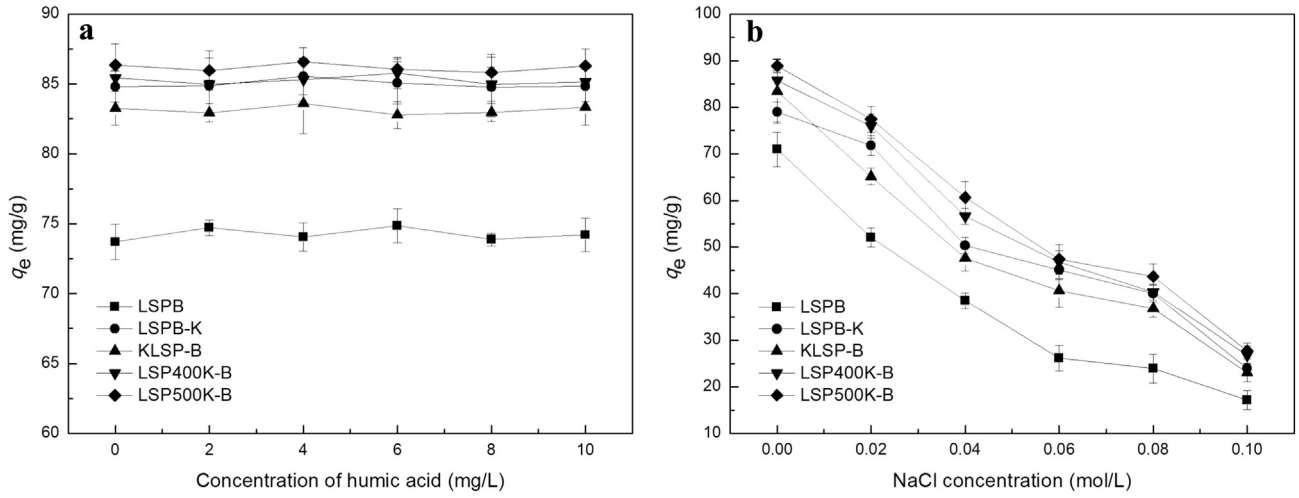

Fig. 8 – Effect of humic acid (a) and ionic strength (b) on E2 adsorption by BCs. Volume 50 mL, adsorbent dose 3 mg, solution concentration 7 mg/L, and agitation speed 160 r/min.

from 4 to 10 is shown in Fig. 7a. The result showed that the adsorption capacity of E2 was stable for all types of BCs when the pH value was 4.0–9.0. It seemed that the pH had little effect on the removal of E2 by the BCs. However, the uptake of E2 by BCs decreased sharply when the pH value increased to about 10.0. A similar tendency can be found in the research of Jiang et al. (2017a). According to their study, the results are very likely to be caused by the characteristic ionization or the micro-species distribution of E2 molecules in aqueous solution. It has been reported that 10.4 is the pK_a of E2 (Lee et al., 2005), which means that deprotonation of E2 would take place around pH 10.0, and then the molecules of E2 would take on a negative charge. As shown in Fig. 7b, the surface charge of the BCs was negative in the pH range of 4.0–10.0. Thus, the electrostatic repulsive interaction was established between negatively charged of E2 anions and BCs, which may explain the lower adsorption capacity observed at pH 10.0 (Jiang et al., 2016). However, there were no corresponding relationships between the surface negative charge of different biochar materials and their uptake of E2 by comparative analysis. This suggested that the electrostatic mechanism might not be the only mechanism for E2 removal by BCs.

2.5. *Effect of humic acid*

Humic acid (HA) constitutes the main part of organic matter in a natural water body, so its influence in the water environment cannot be ignored. Fig. 8a shows that the adsorption capacity of BCs for E2 remained nearly unchanged in the presence of HA (2–10 mg/L). The relatively consistent adsorption performance indicated that the anticipated competitive adsorption behavior between HA and E2 did not appear in this

Table 4 – Comparison of E2 adsorption capacity with other adsorbents.

Different adsorbent	BET surface area (m^2/g)	Experimental conditions			Adsorption capacity (mg/g)	Reference
		pH	Dosage of adsorbents (mg)	C_0 of E2 (mg/L)		
MWCNs	84.3	6.0	100	5	0.47	Al-Khateeb et al. (2014)
CGMG	298.9	7.0	5	2	85.80	Jiang et al. (2017a)
Cattle bone char	114.15	–	–	2	10.12	Patel et al. (2015)
Hydrochar-FMBO	167.17	7.0	5	6	49.77	Ning et al. (2017)
Fe_3O_4/GO	203.72	–	–	10	86.90	Bai et al. (2015)
Rice straw biochar	56.11	–	10	6	26.91	Wang et al. (2017c)
LSPB	25.21	7.0	3	7	75.38	This study
LSPB-K	306.19	7.0	3	7	91.46	This study
KLSP-B	227.20	7.0	3	7	85.75	This study
LSP400K-B	344.42	7.0	3	7	93.05	This study
LSP500K-B	364.30	7.0	3	7	100.60	This study

MWCNs: multi-walled carbon nanotubes; CGMG: β-cyclodextrin/poly supported magnetic graphene oxide; FMBO: Fe-Mn binary oxide; GO: Graphene oxide.
–: data was not found.

system. On one hand, this might be due to the low adsorption ability of HA (HA < 10 mg/L) for E2 (Duan et al., 2019). On the other hand, it could be because of the steric hindrance between the BCs and HA. The relatively complex molecular structures of HA molecules (2 five-member rings, 11 six-member rings, and 17 terminal groups Han et al., 2013) could generate strong steric hindrance for the terminal functional groups to interact with BC active sites (Duan et al., 2019).

2.6. Effect of ionic strength

A series of experiments were performed to test the effect of ionic strength on E2 adsorption by BCs. Different concentrations of NaCl were added into the E2 solutions because it is one of the most common ionic compounds that might exist in industrial sewage. As exhibited in Fig. 8b, the uptake of E2 by BCs decreased with the increase of NaCl concentration. In theory, in such a system the electrostatic forces between the ions of adsorbate and surface of adsorbent are attractive, and the adsorption capacity decreases with the increase of ionic strength. Conversely, in an electrostatic repulsive system, the adsorption capacity will increase with an increase in ionic strength (Aldegs et al., 2008). The other possible explanation of this trend (i.e., adsorption capacity decreasing with the increase of ionic strength) can be attributed to the following points: the infiltration of ions into the diffuse double layer surrounding BC surfaces may lead to the elimination of the repulsive interaction between the adsorbent surfaces and promote the formation of a more compact aggregation structure (i.e., squeezing-out), which is unfavorable for E2 adsorption (Jiang et al., 2016). Therefore, the results suggested that electrostatic attraction between the BC surface and E2 ions and the squeezing-out effect may play important roles in the process of adsorption, and the former might provide further explanation for the high adsorption of E2 by BCs.

2.7. Comparative studies

2.7.1. Comparison between LSP-derived adsorbents

As listed in Table 1, the SA of KOH-activated biochars (LSPB-K, KLSP-B, LSP400K-B and LSP500K-B) were almost 10 times larger than that of raw biochar (LSPB), which confirmed the positive effect of KOH activation on the SA and pore structure of biochar. In addition, the post-treated biochars (LSP400K-B and LSP500K-B) had larger SA than the direct treated biochar (LSPB-K), and the SA of KLSP-B (the pre-treated biochar) was the smallest among KOH-activated biochars. As shown in Table 1, LSPB-K, LSP400K-B and LSP500K-B had higher contents of C, N and H than LSPB, and KLSP-B had the lowest content of C and N. Meanwhile, as shown in the FT-IR spectra in Fig. 4a, three different peaks were presented in the spectrum of KLSP-B before adsorption. The experiment results for activated biochar indicated that the order of KOH activation had a significant impact on material properties, including SA, elemental composition and the FT-IR spectra of samples, which ultimately affected the uptake of E2. Furthermore, the better adsorption capacity of LSP500K-B than LSP400K-B and LSPB-K demonstrated that high-temperature pyrolysis was favorable for adsorption, as it could enhance the SA of biochar. However, the effect of the pyrolysis temperature on elemental composition was relatively small. In general, the E2 adsorption capacity of LSP500K-B was the best, followed by LSP400K-B, LSPB-K, KLSP-B, and LSPB. From the viewpoint of preparation, with its relatively high adsorption and one-step pyrolysis process, the sample LSPB-K showed the advantages of lower energy consumption and simpler process flow than LSP400K-B and LSP500K-B. Therefore, it would make an excellent choice for E2 removal in aqueous solution. From the standpoint of high adsorption efficiency of E2, the best adsorbent choice is LSP500K-B. To obtain better adsorption capacity for E2, optimization of mixture ratios (KOH and biochar) should be explored in further research.

2.7.2. Comparison with other adsorbents

As listed in Table 4, MWCNTs, CGMG, Hydrochar-FMBO, Fe_3O_4/GO, and other biochars (cattle bone char and rice straw biochar) are good potential adsorbents for the removal of E2 from water and their adsorption capacities are 0.47, 85.80, 49.77, 86.90, 10.12, and 26.91 mg/g, respectively. Compared with those materials, the BCs prepared in our study, especially LSP500K-B, showed significantly higher efficiency (100.60 mg/g) for E2 adsorption (initial concentration 7 mg/L) at 290K with low doses, which indicated that the BCs have the potential to remove E2 from water with good efficiency. Therefore, these BCs would provide a new and an effective way for the treatment of E2 in aqueous solution.

2.8. Possible mechanisms

The possible adsorption mechanisms of removal of E2 by BCs were investigated through use of different characterization methods and experiments. Fig. 4 compares the FI-TR spectra for BCs before and after reaction with E2. As shown in Fig. 4b, a peak around 1560 cm^{-1} was observed at LSPB-K, LSP400K-B, and LSP500K-B, which suggested that amine groups were formed on the surface of these three samples. Based on the comparison, it was clear that the peaks at 2969 cm^{-1} of LSPB and 1628 cm^{-1} of LSP500K-B disappeared after E2 adsorption. This observation might be due to the replacement of the aromatic C-H or aromatic ring and bending vibrations of N-H on the carbon surface by E2 species. In addition, a peak around 1380 cm^{-1} (corresponding to the C–H bending of alkyl functional groups) was observed in the spectrum of KLSP-B after reaction with E2, suggesting that E2 had been transferred from the bulk solution onto the active sites of the adsorbent. In addition, the changes of peaks at 1636 and 1620 cm^{-1} might be caused by the π–π interactions between BCs and E2 (Fu et al., 2015; Jiang et al., 2016). According to the studies of adsorption kinetics, chemisorption played an important role in the adsorption process. Isotherm results demonstrated that E2 adsorption by BCs took place at specific homogeneous sites within the adsorbent. Furthermore, pH and ionic strength experiments indicated that electrostatic interaction might play a role in the adsorption process. In short, the adsorption of E2 onto BCs took place through a very complex mechanism involving π–π interactions, chemisorption, monolayer adsorption, and electrostatic interaction.

3. Conclusions

This study demonstrated that BCs are potential adsorbents for the removal of E2 in water. BCs were prepared under laboratory conditions and the LSP500K-B sample was found to have largest SA, 364.30 m^2/g. Studies found that KOH-activated biochars exhibited better adsorption capacity for E2 than raw biochar. Meanwhile, KOH activation and the order of activation steps have great influence on the material. After treatment by KOH, the SA and PV of biochar were significantly improved compared to raw biochar. The post-treated biochars (LSP500K-B and LSP400K-B) showed better adsorption capacity toward E2 than direct-treated biochar (LSPB-K), pre-treated biochar (KLSP-B) and raw biochar (LSPB). In addition, high-temperature-pyrolyzed biochar will be more helpful in E2 removal. External environmental factors (i.e., temperature, pH, and ionic strength) could influence the E2 adsorption capacity of BCs greatly. However, humic acid had little influence on E2 adsorption. Results also showed that chemisorption, π–π interactions, monolayer adsorption and electrostatic interaction might be possible adsorption mechanisms. Further studies are needed to choose better activation parameters, explore other potential activation methods and applications of LSP biochar, and to elucidate the interaction mechanisms between E2 and BCs in greater detail.

Acknowledgments

This work was supported by the National Natural Science Foundation of China (Nos. 51521006, 51609268 and 51809089), the Key Project of Technological Innovation in the Field of Social Development of Hunan Province, China (Nos. 2016SK2010 and 2016SK2001), the Fundamental Research Funds for the Central Universities, and the Natural Science Foundation of Hunan Province, China (Nos. 2018JJ3040 and 2018JJ3096).

Appendix A. Supplementary data

Supplementary data to this article can be found online at https://doi.org/10.1016/j.jes.2019.05.026.

REFERENCES

Abdolhosseinzadeh, S., Asgharzadeh, H., Kim, H.S., 2015. Fast and fully-scalable synthesis of reduced graphene oxide. Sci. Rep. 5, 10160.

Abo-El-Enein, S., Gedamy, Y.H., Ecresh, A., 2017. Nitrate removal from groundwater using sodium alginate doped with nano-hydroxyapatite. Adv. Mater. 6 (6), 102.

Adhikari, S.P., Awasthi, G.P., Lee, J., Park, C.H., Kim, C.S., 2016. Synthesis, characterization, organic compound degradation activity and antimicrobial performance of g-C_3N_4 sheets customized with metal nanoparticle-decorated TiO_2 nanofibers. RSC Adv. 6 (60), 55079–55091.

Ahmad, M., Sangsoo, L., Dou, X.M., Mohan, D., Jwakyung, S., Yang, J.E., et al., 2012. Effects of pyrolysis temperature on soybean Stover and peanut shell-derived biochar properties and TCE adsorption in water. Bioresour. Technol. 118, 536–544.

Ahmad, M., Rajapaksha, A.U., Lim, J.E., Zhang, M., Bolan, N., Mohan, D., et al., 2014. Biochar as a sorbent for contaminant management in soil and water: a review. Chemosphere. 99, 19–33.

Aldegs, Y., Elbarghouthi, M., Elsheikh, A., Walker, G., 2008. Effect of solution pH, ionic strength, and temperature on adsorption behavior of reactive dyes on activated carbon. Dyes Pigments 77 (1), 16–23.

Al-Khateeb, L.A., Obaid, A.Y., Asiri, N.A., Salam, M.A., 2014. Adsorption behavior of estrogenic compounds on carbon nanotubes from aqueous solutions: kinetic and thermodynamic studies. J. Ind. Eng. Chem. 20 (3), 916–924.

Andersson, G.G., Gennip, W.J.H.V., Niemantsverdriet, J.W., Brongersma, H.H., 2002. Calcium induced oxidation of PPV studied with X-ray photoelectron spectroscopy and secondary ion mass spectrometry. Chem. Phys. 278 (2–3), 159–167.

Bai, X., Feng, R.R., Hua, Z.L., Zhou, L.C., Shi, H.C., 2015. Adsorption of 17β-estradiol (E2) and Pb(II) on Fe_3O_4/graphene oxide (Fe_3O_4/GO) nanocomposites. Environ. Eng. Sci. 32 (5), 370–378.

Cheung, W.H., Szeto, Y.S., Mckay, G., 2007. Intraparticle diffusion processes during acid dye adsorption onto chitosan. Bioresour. Technol. 98, 2897–2904.

Duan, Q., Li, X., Wu, Z., Alsaedi, A., Hayat, T., Chen, C., et al., 2019. Adsorption of 17beta-estradiol from aqueous solutions by a novel hierarchically nitrogen-doped porous carbon. J. Colloid Interf. Sci. 533, 700–708.

Dubey, B., 2014. Design and evaluation of proniosomes as drug carrier for ocular delivery of levofloxacin. J. Drug Deliv. Ther. 4 (5), 182–189.

Febrianto, J., Kosasih, A.N., Sunarso, J., Ju, Y.H., Indraswati, N., Ismadji, S., 2009. Equilibrium and kinetic studies in adsorption of heavy metals using biosorbent: a summary of recent studies. J. Hazard. Mater. 162 (2–3), 616–645.

Foo, K.Y., Hameed, B.H., 2010. Insights into the modeling of adsorption isotherm systems. Chem. Eng. J. 156 (1), 2–10.

Fu, J.W., Chen, Z.H., Wang, M.H., Liu, S.J., Zhang, J.H., Zhang, J.N., et al., 2015. Adsorption of methylene blue by a high-efficiency adsorbent (polydopamine microspheres): kinetics, isotherm, thermodynamics and mechanism analysis. Chem. Eng. J. 259, 53–61.

Gorga, M., Insa, S., Petrovic, M., Barceló, D., 2015. Occurrence and spatial distribution of EDCs and related compounds in waters and sediments of Iberian rivers. Sci. Total Environ. 503, 69–86.

Gurushantha, K., Anantharaju, K.S., Renuka, L., Sharma, S.C., Nagawarupa, H.P., Prashantha, S.C., et al., 2017. New green synthesized reduced graphene oxide–ZrO_2 composite as high performance photocatalyst under sunlight. RSC Adv. 7 (21), 12690–12703.

Han, J., Qiu, W., Cao, Z., Hu, J.Y., Gao, W., 2013. Adsorption of ethinylestradiol (EE2) on polyamide 612: molecular modeling and effects of water chemistry. Water Res. 47 (7), 2273–2284.

Huang, H., Tang, J.C., Gao, K., He, R.Z., Zhao, H., Werner, D., 2017. Characterization of KOH modified biochars from different pyrolysis temperatures and enhanced adsorption of antibiotics. RSC Adv. 7 (24), 14640–14648.

Ismagilov, Z.R., Shalagina, A.E., Podyacheva, O.Y., Ischenko, A.V., Kibis, L.S., Boronin, A.I., et al., 2009. Structure and electrical conductivity of nitrogen-doped carbon nanofibers. Carbon 47 (8), 1922–1929.

Janakiraman, N., Johnson, M., 2015. Functional groups of tree ferns (cyathea) using FT-IR: chemotaxonomic implications. Roman. J. Biophysics. 25 (2), 131–141.

Jiang, L.H., Liu, Y.G., Zeng, G.M., Xiao, F.Y., Hu, X.J., Hu, X., et al., 2016. Removal of 17β-estradiol by few-layered graphene oxide nanosheets from aqueous solutions: external influence and adsorption mechanism. Chem. Eng. J. 284, 93–102.

Jiang, L.H., Liu, Y.G., Liu, S.B., Hu, X.J., Zeng, G.M., Hu, X., et al., 2017a. Fabrication of β-cyclodextrin/poly (l-glutamic acid) supported magnetic graphene oxide and its adsorption behavior for 17β-estradiol. Chem. Eng. J. 308, 597–605.

Jiang, L.H., Liu, Y.G., Liu, S.B., Zeng, G.M., Hu, X.J., Hu, X., et al., 2017b. Adsorption of estrogen contaminants by graphene nanomaterials under natural organic matter preloading: comparison to carbon nanotube, biochar, and activated carbon. Environ. Sci. Technol. 51 (11), 6352–6359.

Lee, Y., Yoon, J., Von Gunten, U., 2005. Kinetics of the oxidation of phenols and phenolic endocrine disruptors during water treatment with ferrate (Fe(VI)). Environ. Sci. Technol. 39 (22), 8978–8984.

Li, Z.T., Dvorak, B., Li, X., 2012. Removing 17beta-estradiol from drinking water in a biologically active carbon (BAC) reactor modified from a granular activated carbon (GAC) reactor. Water Res. 46 (9), 2828–2836.

Li, Z.G., Gao, F., Xiao, Z.G., Ao, G.H., Wu, X.Z., Fang, Y., et al., 2015. Synthesis and third-order nonlinear optical properties of a sandwich-type mixed (phthalocyaninato) (schiff-base) triple-decker complexes. Dyes Pigments 119, 70–74.

Li, M.F., Liu, Y.G., Liu, S.B., Shu, D., Zeng, G.M., Hu, X.J., et al., 2017. Cu(II)-influenced adsorption of ciprofloxacin from aqueous solutions by magnetic graphene oxide/nitrilotriacetic acid nanocomposite: competition and enhancement mechanisms. Chem. Eng. J. 319, 219–228.

Li, M.F., Liu, Y.G., Liu, S.B., Zeng, G.M., Hu, X.J., Tan, X.F., et al., 2018. Performance of magnetic graphene oxide/diethylenetriaminepentaacetic acid nanocomposite for the tetracycline and ciprofloxacin adsorption in single and binary systems. J. Colloid Interf. Sci. 521, 150–159.

Liang, Y., Shi, J.W., Xiao, P., He, J., Ni, F., Zhang, J.W., et al., 2018. A lotus-inspired janus hybrid film enabled by interfacial self-assembly and in situ asymmetric modification. Chem. Commun. 54 (91), 12804–12807.

Liu, P., Liu, W.J., Jiang, H., Chen, J.J., Li, W.W., Yu, H.Q., 2012. Modification of biochar derived from fast pyrolysis of biomass and its application in removal of tetracycline from aqueous solution. Bioresour. Technol. 121, 235–240.

Liu, J.F., Lin, G.H., Xiao, C., Xue, Y., Yang, A.K., Ren, H.X., et al., 2015. Sensitive electrochemical immunosensor for α-fetoprotein based on graphene/SnO_2/Au nanocomposite. Biosens. Bioelectron. 71, 82–87.

Morant, C., Andrey, J., Prieto, P., Mendiola, D., Sanz, J.M., Elizalde, E., 2010. XPS characterization of nitrogen-doped carbon nanotubes. Phys. Status Solidi A 203 (6), 1069–1075.

Nakada, N., Nyunoya, H., Nakamura, M., Hara, A., Iguchi, T., Takada, H., 2004. Identification of estrogenic compounds in wastewater effluent. Environ. Toxicol. Chem. 23 (12), 2807–2815.

Ning, Q.M., Liu, Y.G., Liu, S.B., Jiang, L.H., Zeng, G.M., Zeng, Z.W., et al., 2017. Fabrication of hydrochar functionalized Fe-Mn binary oxide nanocomposites: characterization and 17β-estradiol removal. RSC Adv. 7 (59), 37122–37129.

Noir, M.L., Lepeuple, A.S., Guieysse, B., Bo, M., 2007. Selective removal of 17β-estradiol at trace concentration using a molecularly imprinted polymer. Water Res. 41 (12), 2825–2831.

Okpalugo, T.I.T., Papakonstantinou, P., Murphy, H., McLaughlin, J., Brown, N.M.D., 2005. High resolution XPS characterization of chemical functionalised MWCNTs and SWCNTs. Carbon. 43 (1), 153–161.

Özacar, M., Şengil, İ.A., 2005. A kinetic study of metal complex dye sorption onto pine sawdust. Process Biochem. 40 (2), 565–572.

Papageorgiou, S.K., Kouvelos, E.P., Favvas, E.P., Sapalidis, A.A., Romanos, G.E., Katsaros, F.K., 2010. Metal–carboxylate interactions in metal–alginate complexes studied with FTIR spectroscopy. Carbohydr. Res. 345 (4), 469–473.

Patel, S., Han, J., Gao, W., 2015. Sorption of 17β-estradiol from aqueous solutions on to bone char derived from waste cattle bones: kinetics and isotherms. J. Environ. Chem. Eng. 3 (3), 1562–1569.

Pavón, J.M.C., Alonso, E.V., Cordero, M.T.S., Torres, A.G.D., López-Cepero, J.M.L., 2005. Use of spectroscopic techniques for the chemical analysis of biomorphic silicon carbide ceramics. Anal. Chim. Acta 528 (1), 129–134.

Pelch, K.E., Beeman, J.M., Niebruegge, B.A., Winkeler, S.R., Nagel, S. C., 2011. Endocrine-disrupting chemicals (EDCs) in mammals. Hormones and Reproduction of Vertebrates Mammals, pp. 329–371.

Qian, L.B., Zhang, W.Y., Yan, J.C., Han, L., Gao, W.G., Liu, R.Q., et al., 2016. Effective removal of heavy metal by biochar colloids under different pyrolysis temperatures. Bioresour. Technol. 206, 217–224.

Qin, C.Q., Xiao, L., Du, Y.M., Shi, X.W., Chen, J.W., 2002. A new cross-linked quaternized-chitosan resin as the support of borohydride reducing agent. React. Funct. Polym. 50 (2), 165–171.

Regmi, P., Garcia Moscoso, J.L., Kumar, S., Cao, X., Mao, J., Schafran, G., 2012. Removal of copper and cadmium from aqueous solution using switchgrass biochar produced via hydrothermal carbonization process. J. Environ. Manag. 109, 61–69.

Schug, T.T., Janesick, A., Blumberg, B., Heindel, J.J., 2011. Endocrine disrupting chemicals and disease susceptibility. J. Steroid Biochem. Mol. Biol. 127, 204–215.

Shehap, A.M., 2008. Thermal and spectroscopic studies of polyvinyl alcohol/sodium carboxy methyl cellulose blends. Egypt. J. Solids. 31 (1), 75–91.

Shin, K.Y., Hong, J.Y., Jang, J., 2011. Heavy metal ion adsorption behavior in nitrogen-doped magnetic carbon nanoparticles: isotherms and kinetic study. J. Hazard. Mater. 190 (1–3), 36–44.

Sun, W., Zhou, K., 2014. Adsorption of 17β-estradiol by multi-walled carbon nanotubes in natural waters with or without aquatic colloids. Chem. Eng. J. 258, 185–193.

Tan, X.F., Liu, Y.G., Gu, Y.L., Zeng, G.M., Wang, X., Hu, X.J., et al., 2015a. Immobilization of Cd(II) in acid soil amended with different biochars with a long term of incubation. Environ. Sci. Pollut. R. 22 (16), 12597–12604.

Tan, X.F., Liu, Y.G., Zeng, G.M., Wang, X., Hu, X.J., et al., 2015b. Application of biochar for the removal of pollutants from aqueous solutions. Chemosphere. 125, 70–85.

Tan, G.C., Sun, W.L., Xu, Y.R., Wang, H.Y., Nan, X., 2016a. Sorption of mercury(II) and atrazine by biochar, modified biochars and biochar based activated carbon in aqueous solution. Bioresour. Technol. 211, 727–735.

Tan, X.F., Liu, S.B., Liu, Y.G., Gu, Y.L., Zeng, G.M., Cai, X.X., et al., 2016b. One-pot synthesis of carbon supported calcined-Mg/Al layered double hydroxides for antibiotic removal by slow pyrolysis of biomass waste. Sci. Rep. 6, 39691.

Tan, X.F., Liu, Y.G., Gu, Y.L., Xu, Y., Zeng, G.M., Hu, X.J., et al., 2016c. Biochar-basednano-composites for the decontamination of wastewater: a review. Bioresour. Technol. 212, 318–333.

Tan, X.F., Liu, Y.G., Gu, Y.L., Liu, S.B., Zeng, G.M., Cai, X.X., et al., 2016d. Biochar pyrolyzed from MgAl-layered double hydroxides pre-coated ramie biomass (*Boehmeria nivea* (L.) Gaud.): characterization and application for crystal violet removal. J. Environ. Manag. 184, 85–93.

Vijayaraghavan, K., Padmesh, T.V.N., Palanivelu, K., Velan, M., 2006. Biosorption of nickel(II) ions onto *Sargassum wightii*: application of two-parameter and three-parameter isotherm models. J. Hazard. Mater. 133, 304–308.

Wang, T.S., Yu, D.L., Tian, Y.J., Xiao, F.R., He, J.L., Li, D.C., et al., 2001. Cubic-C_3N_4 nanoparticles synthesized in CN_x/TiN_x multilayer films. Chem. Phys. Lett. 334 (1–3), 7–11.

Wang, J., Li, Q., Li, M.M., Chen, T.H., Zhou, Y.F., Yue, Z.B., 2014. Competitive adsorption of heavy metal by extracellular polymeric substances (EPS) extracted from sulfate reducing bacteria. Bioresour. Technol. 163, 374–376.

Wang, P., Li, T., Zhang, D., 2017a. Fabrication of non-wetting surfaces on zinc surface as corrosion barrier. Corros. Sci. 128, 110–119.

Wang, Q., Dölle, K., Tong, J., 2017b. Pharmaceuticals in surface water and waste water treatment plant effluent around the world – a review. Asian J. Environ. Ecol. 3, 1–17.

Wang, X.H., Liu, N., Liu, Y.G., Jiang, L.H., Zeng, G.M., Tan, X.F., et al., 2017c. Adsorption removal of 17β-estradiol from water by rice straw-derived biochar with special attention to pyrolysis temperature and background chemistry. Int. J. Env. Res. Pub. He. 14 (10), 1213.

Weber, W.J.J., Morris, J.C., 1963. Kinetics of adsorption on carbon from solution. J. Sanit. Eng. Divi. 1, 1–2.

Wei, Z., Chen, X., Duan, J., Zhan, G., Wei, Y., Zhang, A., 2019. Branched chain versus straight chain fluorinated surfactant: a comparative study of their anticorrosion performance on carbon steel. J. Mol. Liq. 280, 327–333.

Whitehead, S.A., Rice, S., 2006. Endocrine-disrupting chemicals as modulators of sex steroid synthesis. Best Pract. Res. Clin. Endocrinol. Metab. 20, 45.

Worch, E., 2012. Adsorption Technology in Water Treatment. Walter De Gruyter, Germany Book.

Yan, X., Xu, T., Chen, G., Yang, S., Liu, H., 2004. Study of structure, tribological properties and growth mechanism of DLC and nitrogen-doped DLC films deposited by electrochemical technique. Appl. Surf. Sci. 236 (1–4), 328–335.

Yan, Z.L., Liu, Y.G., Tan, X.F., Liu, S.B., Zeng, G.M., Jiang, L.H., et al., 2017. Immobilization of aqueous and sediment-sorbed ciprofloxacin by stabilized Fe-Mn binary oxide nanoparticles: influencing factors and reaction mechanisms. Chem. Eng. J. 314, 612–621.

Yang, D.X., Velamakanni, A., Bozoklu, G., Park, S.J., Stoller, M.S., Piner, R.D., et al., 2009. Chemical analysis of graphene oxide films after heat and chemical treatments by X-ray photoelectron and micro-Raman spectroscopy. Carbon. 47 (1), 145–152.

Yoon, Y., Westerhoff, P., Snyder, S.A., Esparza, M., 2003. HPLC-fluorescence detection and adsorption of bisphenol A, 17beta-estradiol, and 17alpha-ethynyl estradiol on powdered activated carbon. Water Res. 37 (14), 3530–3537.

Zeng, L., Chen, Y., Zhang, Q., Guo, X., Peng, Y., Xiao, H., et al., 2015. Adsorption of Cd(II), Cu(II) and Ni(II) ions by cross-linking chitosan/rectorite nano-hybrid composite microspheres. Carbohyd. Polym. 130, 333–343.

Zeng, Z.W., Tan, X.F., Liu, Y.G., Tian, S.R., Zeng, G.M., Jiang, L.H., et al., 2018. Comprehensive adsorption studies of doxycycline and ciprofloxacin antibiotics by biochars prepared at different temperatures. Front. Chem. 6, 80.

Zhang, Y.P., Zhou, J.L., 2005. Removal of estrone and 17beta-estradiol from water by adsorption. Water Res. 39 (16), 3991–4003.

Zhang, Z.H., Feng, Y.J., Peng, G., Ce, W., Nanqi, R., 2011a. Occurrence and removal efficiencies of eight EDCs and estrogenicity in a STP. J. Environ. Monit. 13 (5), 1366–1373.

Zhang, G., Zhang, Q., Sun, K., Liu, X., Zheng, W., Zhao, Y., 2011b. Sorption of simazine to corn straw biochars prepared at different pyrolytic temperatures. Environ. Pollut. 159 (10), 2594–2601.

Zhang, W., Mao, S., Chen, H., Huang, L., Qiu, R.L., 2013. Pb(II) and Cr(VI) sorption by biochars pyrolyzed from the municipal wastewater sludge under different heating conditions. Bioresour. Technol. 147, 545–552.

Zhang, F.S., Xie, Y.F., Li, X.W., Wang, D.Y., Yang, L.S., Nie, Z.Q., 2015. Accumulation of steroid hormones in soil and its adjacent aquatic environment from a typical intensive vegetable cultivation of North China. Sci. Total Environ. 538, 423–430.

Zhi, Y.F., Deng, X.F., Ni, Y.H., Zhao, W.B., Jia, Q.M., Shan, S.Y., 2018. Cellulosic Cr(salen) complex as an efficient and recyclable catalyst for copolymerization of SO_2 with epoxide. Carbohyd. polym. 194, 170–176.